# COMPLEX NETWORKS ANALYSIS OF OCEANS' INFLUENCE ON SPRING TIME RAINFALL VARIABILITY OVER SOUTHEASTERN SOUTH AMERICA DURING THE 20th CENTURY

**Verónica Martín-Gómez V[1]. and Marcelo Barreiro[1]**

vero.martin.gomez@gmail.com

[1]Instituto de Física. Universidad de la República, Montevideo (Uruguay).

## Abstract

Southeastern South America (SESA) rainfall presents large variability from interannual to multidecadal times scales and is influenced by the tropical Pacific, Atlantic and Indian oceans. At the same time, these tropical oceans interact among them inducing sea surface temperature anomalies in remote basins through atmospheric and oceanic teleconnections.

In this study we employ a tool from complex network theory to analyze the collective influence of the three tropical oceans on austral spring time precipitation over SESA during the 20th century. We construct a climate network considering as nodes the observed Niño3.4, Tropical North Atlantic (TNA), and Indian Ocean Dipole (IOD) indices, together with an observed or simulated precipitation (PCP) index over SESA. The mean network distance is considered as a measure of synchronization among all these phenomena during the 20th century.

This approach allowed to detect two main synchronization periods characterized by different interactions among the nodes. In particular, the network's nodes that influenced SESA precipitation changed with time. Whereas in the '30s El Niño and the TNA were the main tropical oceanic phenomena that influenced SESA precipitation variability, during the '70s they were El Niño and the IOD. The use of model simulations also allowed to hypothesize the physical mechanism that characterized the interaction among the nodes in the synchronization period.

KEY WORDS: synchronization events, tropical ocean teleconnections, tropic-extratropic teleconnections, precipitation over SESA.

## 1) INTRODUCCIÓN

Southeastern South America (SESA) rainfall variability is influenced by the tropical Pacific, Atlantic and Indian oceans (e.g., Grimm et al., 2000; Barreiro et al., 2010; Yulaeva and Wallace 1994; Silvestri 2004; Mo and Berbery 2011; Chan et al., 2008). At the same time, these tropical oceans interact among them inducing sea surface temperature anomalies in remote basins through atmospheric and oceanic teleconnections (e.g., Enfield and Mayer 1997; Saravannan et al., 2000; Yoo et al., 2013; Annamalai et al., 2003; Wang and Wang 2014). However, nowadays it is not fully understood how these SST anomalies in remote basins interact collectively to influence rainfall variability over SESA and neither how the interaction among the oceans and their influence on SESA precipitation had varied during the last century.

Considering the interaction among oceans and their influence on SESA precipitation variability, we construct a climate network following the methodology of Tsonis *et al*. (2007) and taking different indices that

characterize the tropical oceans: El Niño/Southern Oscillation (Niño3.4), the Tropical North Atlantic (TNA), and the Indian Ocean Dipole (IOD) as well as an index that characterizes precipitation over SESA (PCP) as network's nodes (see Figure 1). We investigate the collective behavior of the network focusing on detection of synchronization events (when the network's nodes are most connected) and how this 'collective-behavior' has evolved with time. The synchronization events are defined considering the mean distance of cross – correlation. Thus, this methodology allows to detect periods when the tropical oceans are more connected and active in influencing rainfall over SESA.

## 2) DATA AND METHODOLOGY

### 2.1. *Data*

We compute the different tropical oceanic indices considering the monthly mean SST data from 1901 to 2005 from ERSSTv3b dataset (Extended Reconstructed Sea Surface Temperature; Smith *et al.*, 2008; and Xue *et al*., 2003) with a resolution of 2º x 2º. The Precipitation index is calculated using the monthly mean observed data during the same period mentioned above from the GPCCv5 dataset (Global Precipitation Climatology Center; Schneider *et al*., 2011) with a resolution of 1º x 1º.

On the other hand, we also consider the simulated precipitation field from an AGCM forced with observed SST. In particular, we use the ICTP-AGCM (Kucharski *et al*., 2006; Molteni F 2003) and construct an ensemble of 9 runs initializing the model with different atmospheric conditions, but all having the same SST as boundary conditions. The precipitation index is considered as the ensemble mean precipitation over the region of interest (see Figure 1) and by construction it will mainly represent the oceanic-forced rainfall variability.

Considering these two types of data we construct two climate networks with the same nodes (represented on Figure 1), but using different types of dataset. In one case we consider observations (the SST from ERSSTv3b and the PCP from GPCCv5), and on the other hand we consider the simulated SST and precipitation data from ICTP-AGCM's outputs. Latter is forced with SST from ERSSTv2. Smith et al., (2008) showed that ERSSTv2 and ERSSTv3 are very similar, and therefore, the main difference in the networks constructed from observed and model data arises due to differences in the evolution of precipitation. We will see below that the network constructed with simulated rainfall can reproduce the observed synchronization and therefore the model's output will allow to study the global circulation anomalies in each synchronization period.

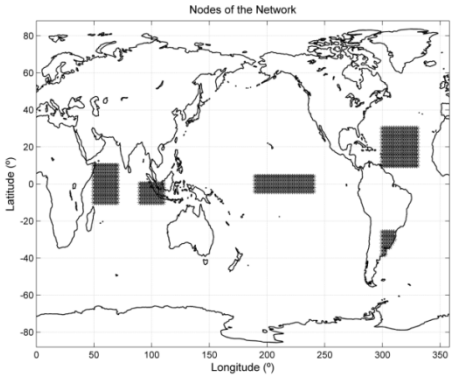


Figure 1. Regions that represents the climate indices: Indian Ocean Dipole (IOD) over the Indian Ocean, Niño3.4 over the central equatorial Pacific Ocean, the Tropical North Atlantic (TNA) and the precipitation over Southeaster South America (PCP).

### *2.2. Methodology*

The methodology consists in several steps:
First, we compute the climate indices by latitudinal and longitudinally averaging SST and precipitation in the different regions considered (Figure 1). We also eliminate the trend of the time series and compute the monthly anomalies removing the climatological cycle from 1901 to 2005. The indices are normalized.

Second, we consider individual trimesters to construct the networks: September – November (SON) for the case of El Niño index and October – December (OND) for the rest of the indices (TNA, IOD and PCP). Therefore, the time series have 105 values, one per year.

SESA precipitation in OND shows large variability on different time scales including interannual to interdecadal (Seager et al., 2010). Also, it is during this season when the teleconnection between Niño3.4 and SESA precipitation is well established and when the IOD takes place and influences SESA precipitation variability (Barreiro *et al.*, 2010; Li *et al*., 2003 and Chan *et al*., 2008). ENSO could induce the SST anomalies in other tropical basins with a lag that varies from 1 to several months. Thus, we established a lag of one month between the Niño3.4 index and the rest of the network nodes to allow the Atlantic and Indian Oceans to respond to the atmospheric anomalies generated from the equatorial Pacific.

Third, following the methodology of Tsonis *et al.* (2007) we construct the network considering the mean network distance as synchronization measure. Mathematically, the mean network distance is defined as:

$$d(t) = \frac{2}{N(N-1)} \sum_{i<j} \sqrt{2\left(1 - \left|\rho_{ij}^{t}\right|\right)} \quad (1)$$

where $t$ denotes the time in the middle of a sliding window of width $\Delta t$=11 years, N represents the number of network's nodes (in this case, 4) and $\rho_{ij}^{t}$ is the correlation coefficient between nodes $i$ and $j$ in the interval [ $t - \frac{\Delta t}{2}$ , $t + \frac{\Delta t}{2}$ ]. The time step for the sliding window is 1 year. The mean network distance as a measure of synchronization is useful to study and describe the variations in the network's topology. Note that the network is completely synchronized when the distance is zero and disconnected when the distance is $\sqrt{2}$ (uncorrelated nodes).

Fourth, to compute the statistical significance of the mean network distance we consider the Montecarlo method employing the following criterion: we first compute the autocorrelation coefficient at lag 1 year of each index (remember that each index has one value per year and represents the seasonal mean), and consider as red noise those with autocorrelation coefficient significant at 95% level in one-tailed t-test (white noise in the opposite case). Following this criterion, only the TNA can be considered as red noise, while the rest of the indices are white noise. Then, we generate 1000 surrogate time series of each index under these null hypotheses and compute the network distance time series considering a sliding window of 11-years length, as done for the observed indices. In this way, we construct 1000 surrogate time series of the mean network distance, which allows determining the 5% level. We consider that there is a statistically significant synchronization event when the mean network distance is below this threshold.

## 3) NETWORK'S TOPOLOGY

The network's topology is studied using the mean network distance time series plotted in Figure 2. The dot and shaded black curve represent the mean network distance computed from observed data (ERSSTv3b and GPCCv5), considering Pearson and Spearman correlation coefficient in equation (1), respectively. The horizontal black line is the threshold level. We found that the network distance is very similar independently on the correlation used except during the last decade of the 20$^{th}$ century, when the network distance computed with Spearman correlation does not show statistically significant synchronization among the network's nodes (Figure 2). This period includes the strong El Niño of 1997 which acts as an outlier strongly influencing Pearson correlation. The similarity in the evolution of both network distances during the first 90 years of the last century suggests that Pearson correlation is a valid measure of interdependence to represent climate teleconnections, and our study will be based on this correlation coefficient.

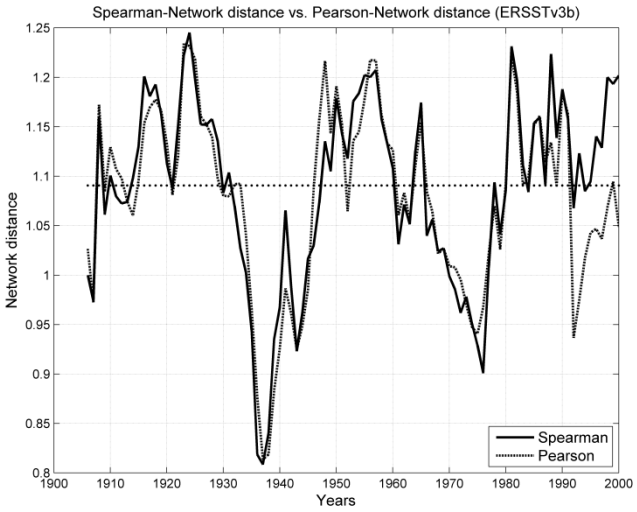


Figure 2. Network distance computed considering Spearman rank (continue line) and Pearson (shaded line) correlations coefficients from ERSSTv3b indices. For each time step, the network distance is calculated considering the definition given by Tsonis *et al*., (2007) and a sliding window of 11 years length. El Niño index in centered on September-October-November (SON), and the rest of the indices on October-November-December (OND).

### *3.1 Variability of the network distance and synchronization periods.*

Figure 3 shows the mean network distance computes considering observed and simulated indices, blue and green curves respectively (observed indices from ERSSTv3b and GPCCv5, and simulated indices from the ICTP-AGCM's outputs). The network distance is characterized by interannual and interdecadal variability, existing three periods in which the observed (blue curve) and simulated (green curve) network distances evolve similarly and present synchronization (mean network distance under the threshold level, Figure 3). Focusing on the observed network distance (blue curve) it is possible to distinguish that the first period occurs from 1933 to 1945 and the second period covers 1966-1978. The last synchronization period (during the '90s) will not be considered since the mean network distance computed using the Spearman correlation does not show synchronization among the network's components (Figure 2, black line).

Overall, looking at Figure 3, the time behavior of the network distance calculated using simulated rainfall (green curve) tends to follow the one constructed with observed rainfall (blue curve). However, while there are periods in which the amplitude of the simulated network distance (green curve) is very similar to that

using observations (blue curve), as can be first synchronization period, there are others in which this is not the case (for example, the second synchronization period). As noted before, the main difference between the observed (blue curve) and simulated (green curve) network distances should arise due to the precipitation index. Whereas in the simulated case the precipitation index contains mainly the oceanically-forced component, the observed precipitation index contains both, the internal variability and oceanically-forced signals. Moreover, model biases may also induce differences between observed and simulated precipitation.

To further analyze the representation of the network distance by the model (green curve), we compute the network distance for each one of the 9 precipitation ensemble members of the experiment and define a confidence interval given by the maximum and minimum values for each 11 years window (grey region on Figure 3). Focusing on the ERSSTv3b-network distance (blue curve on Figure 3), overall the observed network distance falls within the confidence interval except during the first synchronization period, but even then, it is possible to see that the observed and ensemble-mean simulated network distances are very close to each other. A similar situation occurs during 1957-1962. The only point where the behavior could be considered different is 1923 when the observed network distance is out of the confidence interval and does not coincide with the simulated network distance. In any case, it is only one point and one that is not that important for our study because is not within a synchronization period.

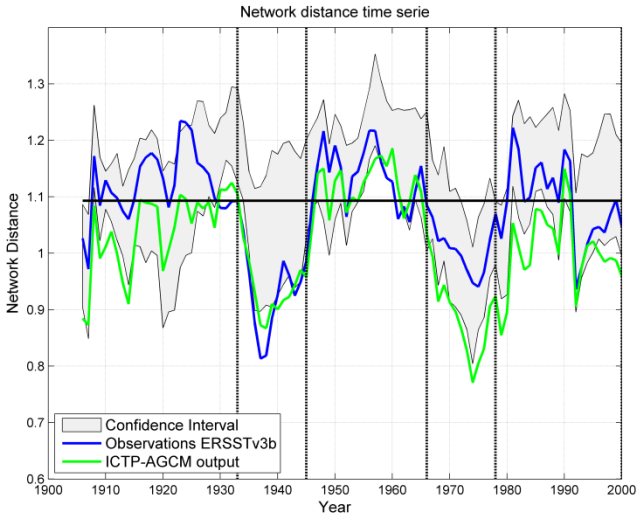


Figure 3. Simulated confidence interval for the network distance time series from 1901 to 2006. The blue and green curves represent the observed and simulated network distance time series respectively. The observed network distance is calculated using SST and PCP from ERSSTv3b and GPCC, respectively to compute the indices. The simulated network distance is obtained considering the SST and PCP from the ICTP-AGCM's outputs. Latter PCP index is the ensemble mean of 9 different experiments.

Figure 3 also shows that in the first (and second) synchronization period the magnitude of the simulated network distance (green line) is just outside the confidence interval, suggesting that large internal atmospheric variability within the ensemble is filtered out in the average procedure. By construction, the simulated network distance (green line) can stay inside or under the confidence interval, but never above. This is because the ensemble mean precipitation index has filtered most of the internal atmospheric variability signal, which would act as noise in the PCP time series decreasing in average the cross-correlation between the PCP index and any of the oceanic indices.

Therefore, the network constructed with simulated rainfall can reproduce the observed synchronization and the model's output will allow to study the global circulation anomalies in each synchronization period.

### *3.2 Node connection during synchronizations.*

Up to this point we have found that during the 20th century there were two synchronization periods: (1933-1945) and (1966-1978). The following step is to determine which nodes had an important role in the network during each period. To address this issue, we compute the Pearson correlation coefficients between each pair of network's nodes (Niño-TNA, Niño-PCP, TNA-PCP, IOD-PCP and TNA-IOD) during each synchronization period using model simulations. We checked the statistical significance considering the 95% level in a Monte Carlo Method based on the generation of 10000 surrogate time series.

During the '30s, Niño3.4 is connected to all the rest of the nodes and there is a link between PCP and TNA (correlation values computed not shown). During the '70s, Niño3.4 is also connected to all the nodes, but the link PCP becomes connected to the IOD (correlation values computed not shown). From the point of view of precipitation over SESA, during the '30s the equatorial Pacific and the tropical north Atlantic dominated the oceanically-forced component of the variability. On the other hand, during the '70s the TNA does not play a role, and the Indian ocean becomes connected to rainfall over SESA, in addition to the Pacific. This result can also be observed in Figures 4 (a) and (c), which represent the correlation map between the PCP index and the sea surface temperature anomalous field in each synchronization period, indicating the regions of the ocean that influence rainfall variability over Southeastern South America.

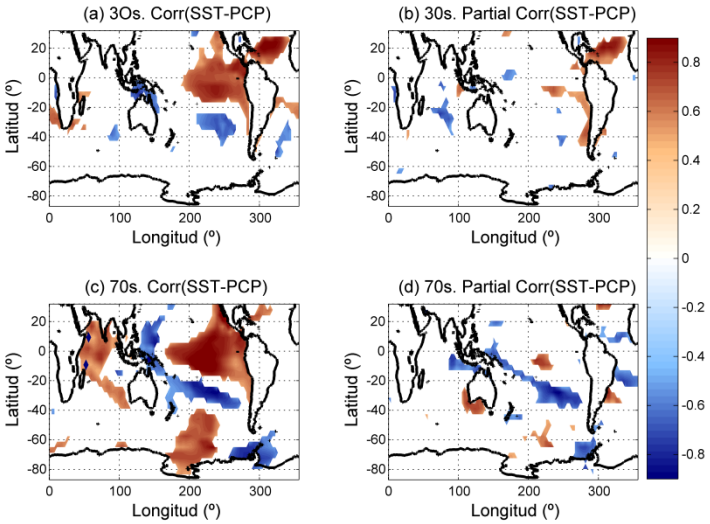


Figure 4. Correlation maps between precipitation index (OND) and the sea surface temperatures anomalies centered on OND: (A) in the 30s and (C) in the 70s. Partial cross correlation maps between precipitation index (OND) and the sea surface temperatures anomalies centered on OND maintaining El Niño3.4 index (SON) constant: (B) in the 30s and (D) in the 70s in the 90s. These maps were computed considering ICTP-AGCM output. Shown values exceed 95% level of confidence from one tailed t-test.

In the following section we hypothesize the possible physical mechanisms that characterized the interaction among the nodes of the network important for rainfall over SESA based on the literature. We employ the ICTP-AGCM's output since as we saw, this model reproduces well the observations and allows to better characterize the oceanically-forced atmospheric circulation anomalies.

## 4) DISCUSSION

### *4.1. Period (1933-1945).*

The oceanic nodes that had an important role on rainfall variability during the period 1933-1945 are Niño3.4, the Tropical North Atlantic (TNA).

There are two different processes through which a warm anomaly in the equatorial Pacific can influence the TNA: a weakening of the trades which decreases the oceanic heat loss (e.g. Enfield and Mayer, 1997) and the tropospheric temperature warming bridge (Chiang and Sobel, 2002). The regression maps onto Niño3.4 show a small warming of the tropical north Atlantic accompanied by weak decreased trades (Figures 5 (a) and (c)). The small TNA response might be consequence of the small lag time allowed for the ocean response (1 month), instead of a typical scale of one season (e.g. Enfield and Mayer, 1997; Saravanan *et al*., 2000).

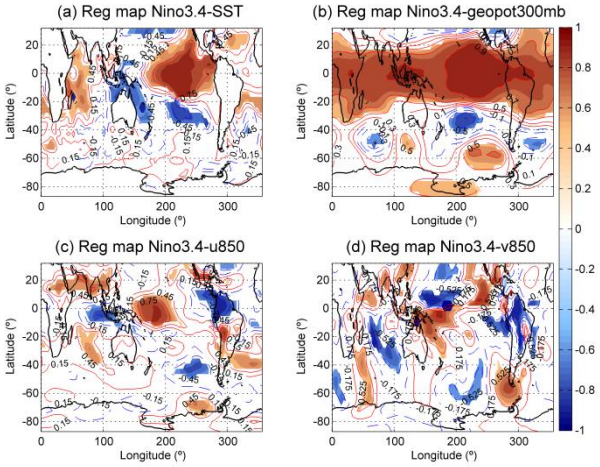


Figure 5. Regression map of the El Niño3.4 index (centered on SON) with: (a) sea surface temperatures anomalies, (b) geopotential height 300mb (geopot300mb), (c): zonal wind anomalies in 850mb (u850) and (d) meridional wind in 850mb (v850). The SST, geopot300, u850 and v850 are centered on OND. Period (1933-1945). Shaded regions represent values higher than 95% confidence level for one tailed t-test. Maps computed from the ICTP-AGCM outputs.

The mechanisms through which El Niño influences SESA involve both upper and lower level atmospheric circulation anomalies. In upper levels the Rossby wave trains propagating from the equatorial Pacific increase the baroclinicity and the advection of cyclonic vorticity over the region (Yulaeva and Wallace, 1994; Grimm *et al*., 2000). This can be observed in the regression map of the geopotential height onto the El Niño3.4 index (Figure 5 (b)), which shows the presence of a through-ridge system over subtropical South America. At the same time, in lower levels there is an increase of the northerly transport of moisture into the region because of a strengthening of the southward wind (Figure 5 (d), in agreement with Silvestri, 2004). The combination of these two factors favors an increase of the precipitation over SESA.

Regarding the interaction between the TNA and PCP, it is important to note that the correlation is approximately 0.9, larger than between PCP and Niño3.4. Also even when El Niño signal is removed (Figure 4 (b)), the SST anomaly in the TNA is still significantly correlated with rainfall over SESA. This suggests that the link between TNA and PCP is direct and that the SST anomalies in the TNA cannot be completely explained by ENSO forcing. To look at the influence of TNA directly onto SESA we performed partial regression maps of geopotential height in 300mb and meridional wind in 850mb onto the TNA index maintaining Niño3.4 index constant (Figures not shown). We found that in upper levels the geopotential height shows a through over SESA favoring the ascent motions over this region. At the same time, in lower

levels there is an increase of the southward winds, and therefore, of the northerly transport of moisture. However, the changes in the meridional wind component and the advection of cyclonic vorticity over the region are not significant and further work is needed to understand the influence of the TNA on rainfall over SESA.

### *4.2. Period (1966-1978).*

In this case, the oceanic nodes that had an important role on rainfall variability are the Niño3.4 and the Indian Ocean Dipole.

The interaction between El Niño and the precipitation over SESA is similar to the previous case since the two favorable conditions to the increase of the precipitation over the region of study are present again (Figures 6 (b) and (d)).

In this period the Indian Ocean Dipole appears like an important network's node, having a significantly link with the precipitation over Southeastern South America (Figure 4 (c)). This link would suggest an influence of the Indian Ocean to the rainfall over SESA. However the partial cross - correlation map between the precipitation index and the sea surface temperatures field maintaining the El Niño3.4 index constant (Figure 4 (d)), shows that the correlation between the PCP and SST over the Indian Ocean becomes not significant, suggesting that the appearance of this link could be due to the fact that both nodes have a common forcing: El Niño. Another possibility is that the Indian Ocean warming, as consequence of the Pacific forcing, influenced the rainfall over SESA through the eastward propagation of Rossby waves, mechanism already proposed by Saji *et al*., (2005) and Chan *et al*., (2008). In fact, the regression map of 300mb geopotential height shows significant anomalies in the southeastern Indian Ocean and the extratropical atmosphere (Figure 6 (b)) that were barely present in the ‘30s (Figure 5 (b)). These Rossby wave trains may interact with the Rossby wave train forced by the tropical Pacific, and together may favor better conditions for increased precipitation over SESA (in agreement with the previous works of Saji *et al*., (2005) and Chan *et al*., (2008)).

The connection between both oceans (equatorial Pacific and Indian) is established through anomalous winds (Wang and Wang, 2014). During the 70s, the regression map of the Niño3.4 index and the 850mb zonal wind (Figure 6(c)) shows negative anomalies of the zonal wind over the western shore of Sumatra that favors upwelling and contributes to decreasing the SST, and positive anomalies over the Arabian Sea and Bay of Bengal facilitating the homogeneous increase of the SST there. Nevertheless, during this period the Indian Ocean warms rather homogeneously presenting a weak east-west SST gradient (Figure 6 (a)).

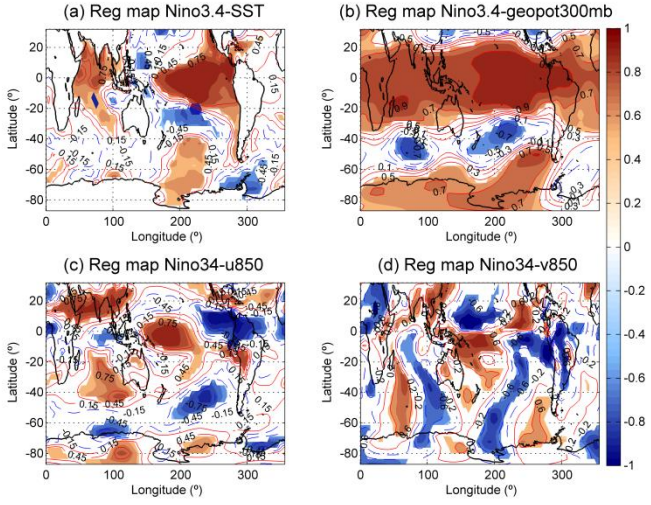

Figure 6. Regression map of the El Niño3.4 index (centered on SON) with: (a) sea surface temperatures anomalies, (b) geopotential height 300mb (geopot300mb), (c) zonal wind anomalies in 850mb (u850) and (d) meridional wind in 850mb (v850). The SST, geopot300, u850 and v850 are centered on OND. Period (1966-1978). Shaded regions represent values higher than 95% confidence level for one tailed t-test. Maps computed from the ICTP-AGCM outputs.

## 5) SUMMARY

Following the methodology of Tsonis *et al*., (2007) we have constructed a network considering as nodes three oceans indices that characterize the interannual variability of the tropical oceans (Niño3.4, IOD and TNA) as well as an index that characterizes the precipitation over Southeastern South America (PCP). We studied the network's topology and the collective behavior of the nodes through the detection of synchronization events considering the mean network distance as a measure of synchronization among the nodes.

The main results of the study are as follows:

Overall, we were able to show that the network distance presents interannual and interdecadal variability and that there were the two synchronizations periods during the last century. The first is from 1933 to 1945 (30s) and the second covers 1966-1978 (70s). A third potential synchronization period was detected during the '90s, but depends on the correlation measured used and is not further studied.

The connectivity among the nodes in the network changed with time. Moreover, whereas in the first synchronization period the nodes which influence SESA precipitation were El Niño and the TNA, in the second period were El Niño and the IOD.

During the two synchronization periods El Niño phenomenon increases the precipitation over Southeastern South America. This result is in agreement with previous studies and might be understood through an increase of the northerly transport of moisture in lower levels and the advection of cyclonic vorticity in upper levels (in agreement with Silvestri *et al*., (2004), Yulaeva and Wallace, (1994) and Grimm *et al*., (2000)).

Regarding the interaction between the TNA and PCP during the 30s, it is important to note that even after El Niño signal is removed, the TNA is significantly correlated with rainfall over SESA. This suggests that the link between TNA and PCP is direct and the SST anomalies in the TNA cannot be completely explained by ENSO forcing.

There are two possible, not mutually exclusive ways, of interpreting the interaction between the IOD and PCP. One possibility is that the appearance of this link is due to the fact that both nodes (IOD and PCP) have a common forcing: El Niño. Another possibility is that the Indian Ocean warming influences rainfall over Southeastern South America through the eastward propagation of Rossby waves (in agreement Saji *et al*., (2005) and Chan *et al*., (2008)). This Rossby wave train could interact with the Rossby wave train forced by the tropical Pacific and together may favor better conditions for increased precipitation over SESA.

Our results suggest a complex dynamics among the tropical oceans and their influence on rainfall over SESA that varies on interannual and interdecadal time scales. The complex network perspective used here has allowed to gain new insights in their collective behavior, and resulted in new questions that need to be addressed in future studies.

## REFERENCES

Annamalai H, Murtugudde R, Potemra J, Xie SP, Liu P, Wang B. 2003. Coupled dynamics over the Indian Ocean: spring initiation of the zonal mode. *Deep Sea Research II:Tropical Studies in Oceanography*, **50**(12): 2305-2330.

Barreiro M. 2010: Influence of ENSO and South Atlantic Ocean on climate predictability over southeastern South America. *Climate dynamics **35**: 1493-1508.* DOI: 10.1007/s00382-0666-9

Chan SC, Behera SK, Yamagata T. 2008. Indian Ocean Dipole influence on South American rainfall. *Geophysical Research Letters* **35**(14). DOI: 10.1029/2008GL034204.

Chang P, Fang Y, Saravanan R, Ji L, Seidel H. 2006. The cause of the fragile relationship between the Pacific El Niño and the Atlantic Niño. *Nature*, **443**: 324-328. DOI:10.1038/nature05053.

Chiang JC, Sobel AH. 2002. Tropical tropospheric temperature variations caused by ENSO and their influence on the remote tropical climate. *Journal of Climate* **15:** 2616-2631.

Duchon CE. 1979: Lanczos Filtering in One and Two Dimensions. *Journal of Applied Meteorology.***18:**1016–1022.

Enfield DB, Mayer DA. 1997. Tropical Atlantic sea surface temperature variability and its relation to El Niño Southern Oscillation. *Journal of Geophysical Research: Oceans.* **102**: 929-945. DOI: 10.1029/96JC03296.

Grimm AM, Barros VR, Doyle ME. 2000. Climate variability in Southern South America associated with El Niño and La Niña events. *Journal of Climate* **13**(1): 35-58.

Kucharski F, Molteni F, and Bracco A. 2006. Decadal interactions between the western tropical Pacific and the North Atlantic Oscillation. *Climate dynamics* **26**: 79-91.

Li T, Wang B, Chang CP, Zhang Y. 2003. A Theory for the Indian Ocean Dipole-Zonal Mode. *Journal of the Atmospheric Science* **60**: 2119-2137.

Mo KC, Berbery EH, 2011. Drought and Persistence Wet Spells over South America Base on Observation and the U.S. CLIVAR Drought Experiments. *Journal of Climate*. **24**: 1801-1820. DOI: 10.1175/JCI3874.1

Molteni F. 2003. Atmospheric simulations using a GCM with simplified physical parameterizations. I: Model climatology and variability in multi-decadal experiments. *Climate Dynamics* **20**: 175-191.

Saji NH, Ambrizzi T, Ferraz SET. 2005. Indian Ocean Dipole mode events and austral surface air temperature anomalies. *Dynamics of Atmospheres and Oceans* **39**:87-101.

Saravanan R, and Chang P. 2000. Interaction between Tropical Atlantic Variability and El Niño – Southern Oscillation. *Journal of Climate* **13**: 2177-2194.

Schneider U, Becker A, Finger P; Meyer-Christoffer A, Rudolf B, Bruno; Ziese M. 2011. GPCC Full Data Reanalysis Version 6.0 at 1.0: Monthly Land-Surface Precipitation from Rain-Gauges built on GTS-based and Historic Data. DOI: 10.5676/DWD_GPCC/FD_M_V6_100.

Seager R, Naik N, Baethgen W, Robertson A, Kushnir Y, Nakamura J, Jurburg S. 2010. Tropical Oceanic Causes of Interannual to Multidecadal Precipitation Variability in Southeast South America over the past Century. *Journal of Climate*. 23: 5517-5539. Doi: 10.1175/2010JCLI3578.1.

Silvestri GE. 2004. El Niño signal variability in the precipitation over southeastern South America during the austral summer. *Geophysical Research Letters* **31**(18). DOI: 10.1029/2004GL020590.

Smith TM, Reynolds RW, Peterson TC, Lawrimore J. 2008. Improvements to NOAA's Historical Merged Land-Ocean Surface Temperature Analysis (1880-2006). *Journal of Climate.*, **21,** 2283-2296.

Tsonis AA, Swanson K, Kravtsov S. 2007. A new dynamical mechanism for major climate shifts. *Geophysical Research Letters* **34**(13): L13705. DOI: 10.1029/2007GL030288.

Wang X, and Wang C. 2014. Different impacts of various El Niño events on the Indian Ocean Dipole. *Climate dynamics* **42**: 991-1005

Xue, Y, Smith TM, Reynolds RW. 2003. Interdecadal changes of 30-yr SST normal during 1871-2000 *Journal of Climate*, **16**, 1601-1612.

Yoo GH, Kug JS, Park JY, Jin FF. 2013. Sea surface temperature in the north tropical Atlantic as a trigger for El Niño/Southern Oscillation events. *Nature Geoscience* 6:112-116. Doi: 10.1038/NGEO1986.

Yulaeva E, Wallace JM. 1994. The signature of the ENSO in global temperature precipitation fields derived from the Microwave Sounding Unit. *Journal of Climate* **7**:1719-1736.